THE DESIGN and PERFORMANCE of DIGITAL CONTROL LAWS for ADVANCED AIRCRAFT HYDRAULIC ACTUATION SYSTEMS

ICAS-94-7.7.4

Louis H. L. Chun and David A. Cowling
Department of Aerospace Engineering, University of Bristol, Bristol, BS8 1TR, U.K.

This paper examines alternative controller design approaches which use digital loop closure to increase the bandwidth and reduce the phase lag at low frequency of an actuation system. The methods have been evaluated on a hydraulic system test bench for a Jaguar fly-by-wire taileron actuation system. The results show that the above objectives have been achieved and there is no sign of any lack of robustness. However, the impedance simulation indicate that the digital controller, pole-assignment plus Kalman filter, would produce an impedance that is less stiff than the original as seen when under analogue control.

Nomenclature

C_f valve flow coefficient
$\mathbf{C}$ output matrix
$\mathbf{C}_1$ controller output matrix
d_o viscous damping
$D(s)$ compensator in s-domain
$D(z)$ compensator in z-domain
$D(z)$ compensators in z-domain
F_E external force
G_{mv} main valve gain
G_{sv} servovalve gain
G_{IL} inner loop gain
G_{MR} main ram gain
G_{OL} outer loop gain
G_1 error gain
$G(s)$ transfer function in s-domain
$G_i(s)$ transfer functions in s-domain, (i = 1..3)
i $\sqrt{-1}$
K compensator gain
$\mathbf{K}$ control law matrix $[K_1\ K_2\ K_3\ K_4]$
$\mathbf{L}_\infty$ steady-state Kalman gain matrix
N input scaling factor
$P(s),Q(s)$ polynomials
$\mathbf{Q}_w$ spectral density matrix of $\mathbf{w}$
$\mathbf{R}_v$ spectral density matrix of $\mathbf{v}$
T sampling rate
T_{iA} time constants, (i = 1..4)
u input signal
$\mathbf{v}$ measurement noise
$\mathbf{w}$ process noise
$\mathbf{x}$ state vector $\left[x_{mv}\quad \ddot{x}_o\quad \dot{x}_o\quad x_p\right]^T$
$\bar{\mathbf{x}}, \hat{\mathbf{x}}$ current and estimate states of Kalman filter
X_i input demand
X_l output structure displacement
X_o inertia load displacement
X_p main ram displacement
X_s main ram body displacement
X_{mv} main valve displacement
X_{sv} servovalve displacement
$\mathbf{y}$ output matrix
$\mathbf{y}_1$ measurable output matrix
Γ discrete plant control input matrix
ζ damping ratio
ζ_c damping ratio of control surface vibration mode
Φ discrete plant system matrix
ω_c resonant frequency

Introduction

Many modern high performance aircraft employ high gain manoeuvre demand systems to improve their stability and pilot handling qualities. The frequency response of the primary actuation systems used in such aircraft is of crucial importance. Phase lags at low frequency can influence the pilot handling qualities, while high bandwidth is required to minimize the impact of the actuator on the gain and phase margin of the flight control system. Typically such actuators employ proportional feedback of the control valve and main ram to achieve the desired closed-loop performance. However, the inclusion of compensators such as lead-lag filters may be required to improve the frequency response.

The concept of the fly-by-wire (FBW) flight control systems has lead to the new generation of flight control

technologies such as computer-controlled, self-contained actuators incorporated in digital avionics systems. By taking the advantage of increasing sophistication and flexibility of digital processors, the majority of control and command computations can be performed within the actuator module. Thus the flight control computer (FCC) is only responsible for the commanded positions of control surfaces. Sophisticated computing facilities, dedicated to an actuator, not only allow for the application of more complex control schemes, but also facilitate the implementation of other functions such as on-line monitoring systems.

The achievable bandwidth of an actuator using conventional loop closure techniques may be limited by the resonance of the control surface inertia against the actuator hydraulic stiffness and the structural stiffnesses. In current practice, actuation systems are designed so that their bandwidth is below the resonant frequency. This in turn limits the scope for increasing the bandwidth and minimizing the phase lag at low frequency.

In this paper the alternatives to conventional loop closure have been evaluated on a Jaguar FBW hydraulic actuation system incorporating a representation of the control surface resonance effects. The design and performance of the digital controllers for the actuation system will be presented in the following sections.

Rig Description

Jaguar FBW Actuator

In this research, the Jaguar FBW actuator is mounted on a test rig as shown in Figure 1. An inertia load is driven by the actuator output through a lever assembly and an output stiffness link assembly. The line of action of the main ram piston force is offset from the centre of rotation of the inertia load.

This actuation system is operated by a hydraulic power unit and an electronics control cabinet. A schematic diagram of the hydraulic circuit is depicted as in Figure 2. The hydraulic control panel and the power unit are connected by two flexible hoses which are cut to a suitable length in order to minimize the fluid line dynamics.[1]-[3] An accumulator is also fitted to the hydraulic control panel's supply line to smooth out supply pressure fluctuations as the flow demand increases.

Electronics Cabinet

Figure 3 is a schematic diagram of the electronics cabinet which is used to control the actuator and to measure the required parameters for model validations.[4]-[6] The original inner and outer loop analogue signals are fed back from the main valve LVDTs and main ram LVDTs respectively. The forward control path carries the error signal obtained when the external input is summed with the outer loop feedback and inner loop feedback. The error signal is then amplified to drive the electrohydraulic servovalves. In order to investigate the performance and benefits of digital loop closure, the Jaguar FBW actuation is analysed as a single-input/single-output (SISO) system or a single-input/multi-loop output system. The electronics cabinet was reconfigured in such a way that the actuator could be controlled by a digital computer.

Data Acquisition and Control

The computer used to control the actuator is an 80386 IBM compatible with a speed of 33 MHz suitable for the DT2801-A and DT2824-PGH plug-in boards which can be addressed by the microcomputer as memory locations. The configuration of the hardware is 16-channel, A/D and D/A bipolar, single-ended and ±10 V full scale.

Figure 4 depicts the configuration for the SISO and single-input/multi-loop output systems. The digital computer (controller) forms part of the control of the process. The boards form the interface between the digital analogue inputs and outputs. The computer closing the control loop is programmed with digital control algorithms, by means of which new control signals are determined using one or more of the measured values and the desired values, in order to achieve a particular control objective. The speed of analogue conversions is very critical so that Direct Memory Access (DMA) is used for control. More details of the boards and their programming and control are given in Data Translation User manual.[7]

Description of the Jaguar FBW Actuation System

Figure 5 shows schematically the Jaguar FBW taileron actuation system with an equivalent inertia load attached to the ram. This system is a duo-triplex type in which two independent hydraulic systems drive a tandem-ram arrangement. In the tandem-ram arrangement of the Jaguar FBW actuator, hydraulic system No.1 has unequal piston areas, while system No.2 has equal areas. The main control valves are driven by hydraulic flows from six electrically driven flapper nozzle servovalves, three for each system. The main control valve is actuated by a summing flange, which is moved by the force produced by opposing pistons supplied from the control ports of each servovalve. An interconnecting link joins the two main control valve spools so as to ensure that their flanges move in unison to control the tandem ram.

On the test rig used for evaluation of the control laws described in this paper, the main ram moves the

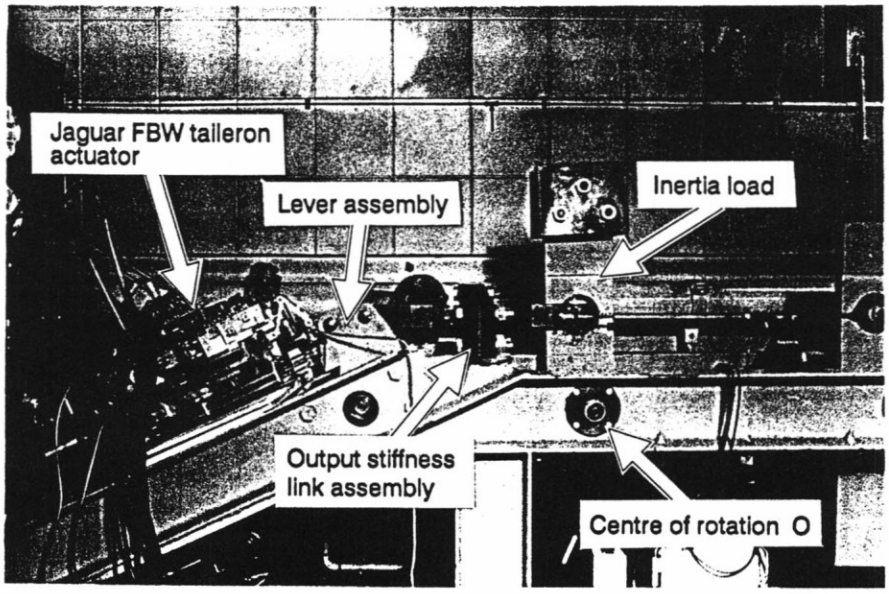

Figure 1 Taileron fly-by-wire actuator mounted on test rig

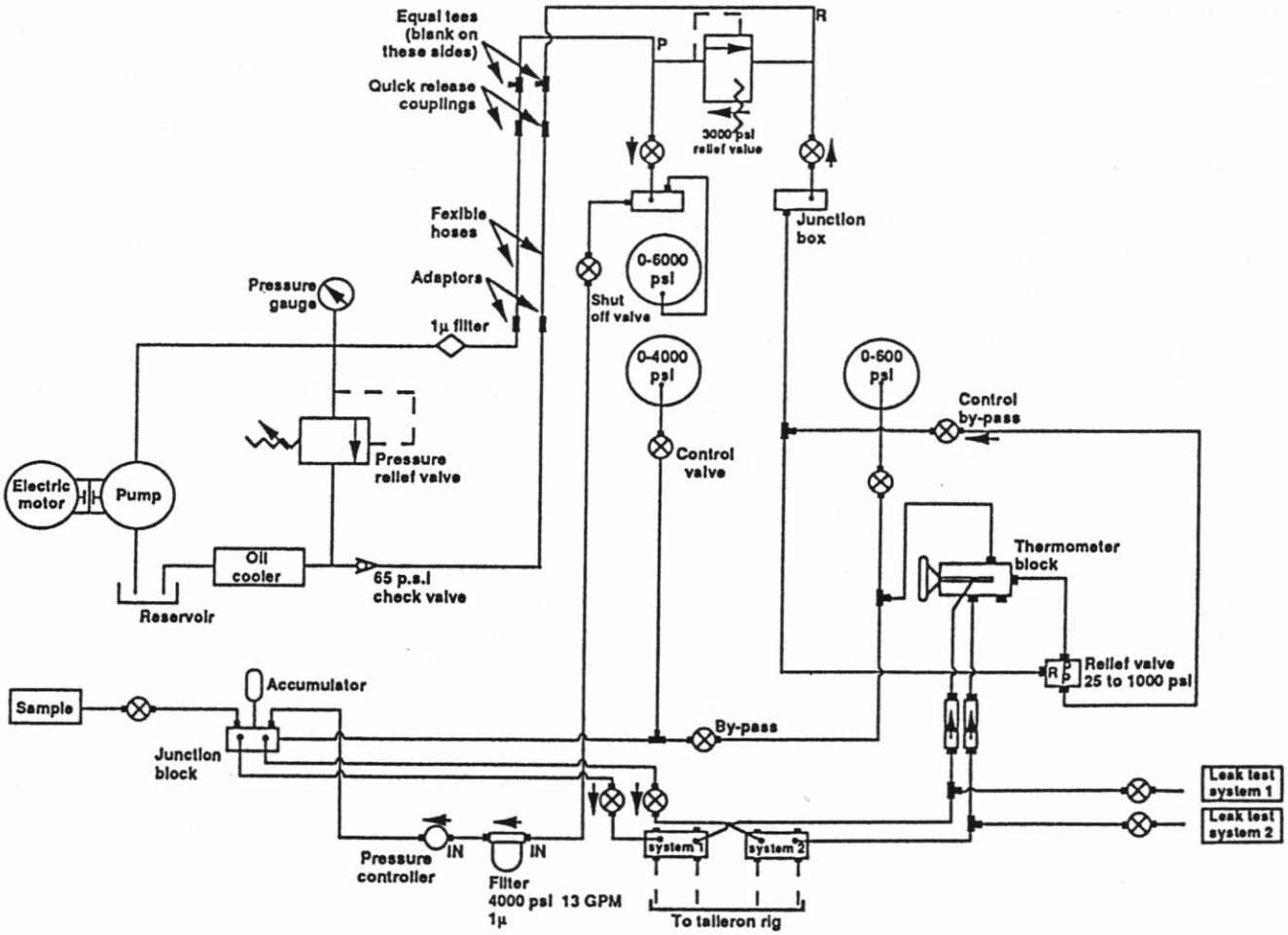

Figure 2 Schematic diagram of hydraulic circuit

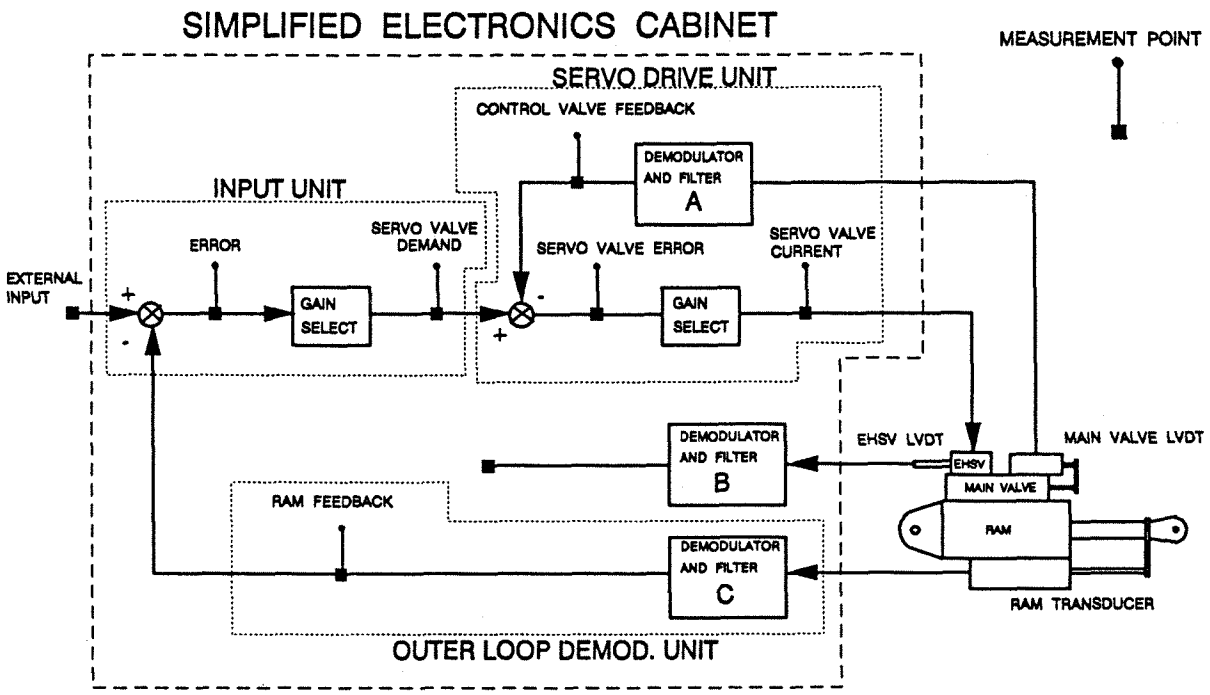

Figure 3 Block diagram of electronics cabinet

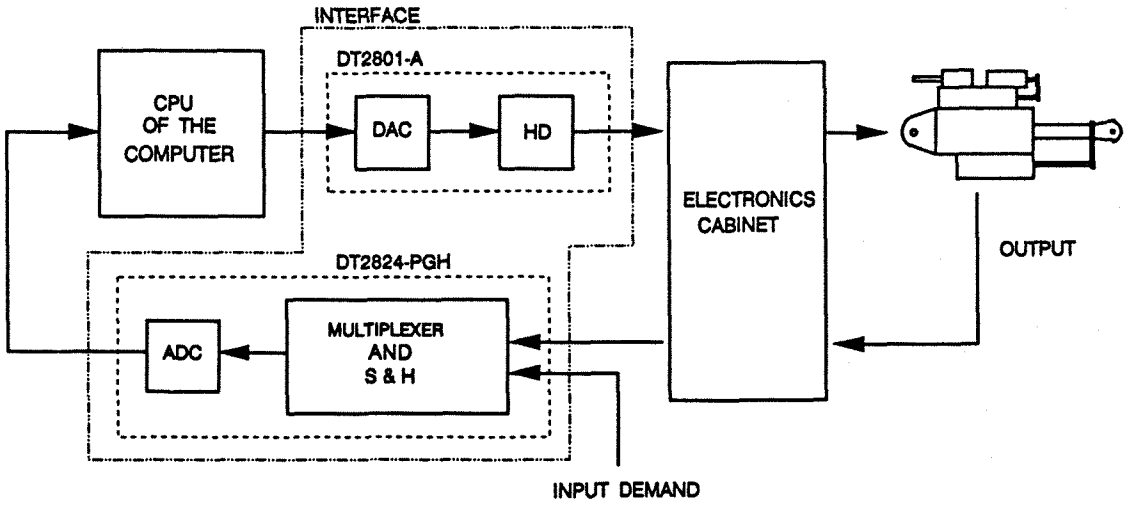

Figure 4 Digital loop closure of the Jaguar fly-by-wire actuation system

inertia load connected by a stiffness representing the structural characteristics of the control surface. This arrangement provides a representation of the vibration mode resulting from the inertia acting against the hydraulic stiffness and the aircraft structural stiffnesses. The actuator body is connected to earth through a stiffness representing the back-up structure of the installation in the airframe. A damper connected between the inertia and earth is included in the mathematical modelling of the actuation system and is shown in the figure for clarification.

System Modelling

In order to investigate the control law design for the actuation system, both linear and nonlinear mathematical models have been formulated. The full description of the model development and validation has been carried out.[4]-[6] The work discussed in this paper emphasises the design of control laws using the linear model as shown schematically in Figure 6. In this model, the servovalve is modelled as a gain and a first order lag, whereas the main valve dynamics are modelled as a gain and an integrator. The model of the main ram dynamics includes the pressures and fluid compressibility in the chambers. The displacements of the control surface and the main ram can be described in terms of the main valve displacement by two transfer functions with the same denominator term. For convenience the block diagram shows two rational transfer functions in series, although the state-space implementation of the model utilised a single set of equations.

The feedback loops as depicted in Figure 6 show an inner loop feedback of the main valve position and an outer loop feedback of the main ram position. In practice the existing Jaguar FBW actuation system has the outer loop closed by the main FCC.[8]

Digital Control Design of the Actuation System Using Pole-zero Cancellation

One straightforward approach to overcoming the problems associated with the control surface resonance is to cancel the dynamics of this mode within the forward loop. This can be achieved by using a compensator to cancel the control surface resonance and introduce new poles in more desirable locations.

In this design it is assumed that there are no electrical and hydraulic failures. The original specification for the actuation system requires gain and phase margins of ≥6 dB and ≥50° respectively. The first part of the compensator design procedure is accomplished in the continuous time domain using the root-locus and Bode methods to derive a satisfactory compensator $D(s)$.[9],[10] This is then converted to an equivalent $D(z)$ by applying the theory and techniques of discretization.[11]

The actuation system as shown in Figure 6 can be compensated by replacing the outer loop gain G_{OL} by a compensator $D(s)$. Before designing the compensator $D(s)$ using pole-zero cancellation, it is appropriate to make certain simplifying assumptions:

1. the bandwidths of the servovalve lag and inner loop feedback filter are high so that their transfer functions can be considered to be equal to 1,

2. outer loop anti-aliasing filter can be taken out since its bandwidth is larger than the system bandwidth,

3. since the sampling rate is at least 200 Hz, the lagging effect can be considered to be negligibly small and any approximation to digital effects such as a Padé approximations can be neglected.

The simplified block diagram including the compensator is illustrated in Figure 7. Since the main ram displacement is used for feedback, the uncompensated system consists of four open-loop poles, including a pair of complex-conjugate poles, and a pair of open-loop complex-conjugate zeros. With two hydraulic lanes operating, the transfer functions of the inner loop and main ram dynamics are respectively

$$G_1(s) = \frac{0.0203}{s + 160.23} \tag{1}$$

$$G_2(s) = \frac{50(s^2 + 28.64s + 53879.69)}{s(s^2 + 28.64s + 41857.79)} \tag{2}$$

Hence the four open-loop poles are s = 0, -160.23, -14.3±204.09i and two open-loop zeros s = -14.32±232.12i. The transfer function of the compensator is chosen to be

$$D(s) = \frac{K(s^2 + 28.64s + 41857.79)}{s^2 + 200s + 20000} \tag{3}$$

where K is the gain of the compensator. The complex-conjugate zeros of the compensator cancel the complex-conjugate poles of the main ram dynamics. The roots of the compensator insert a new pair of complex-conjugate poles s = -100±100i. Referring to Figure 7, when the feedback of the main ram position is closed, the transfer function of X_p/X_i is

$$\frac{X_p}{X_i}(s) = \frac{D(s)G_1(s)G_2(s)}{1 + D(s)G_1(s)G_2(s)} \tag{4}$$

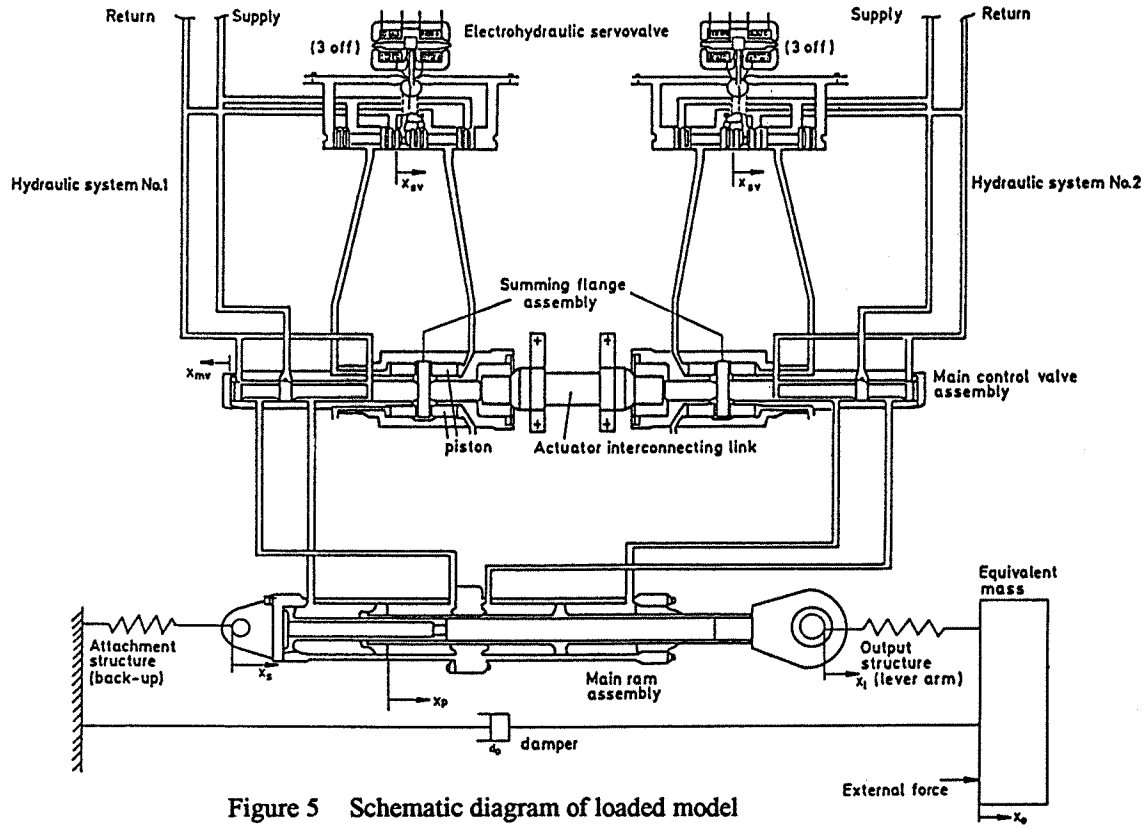

Figure 5 Schematic diagram of loaded model

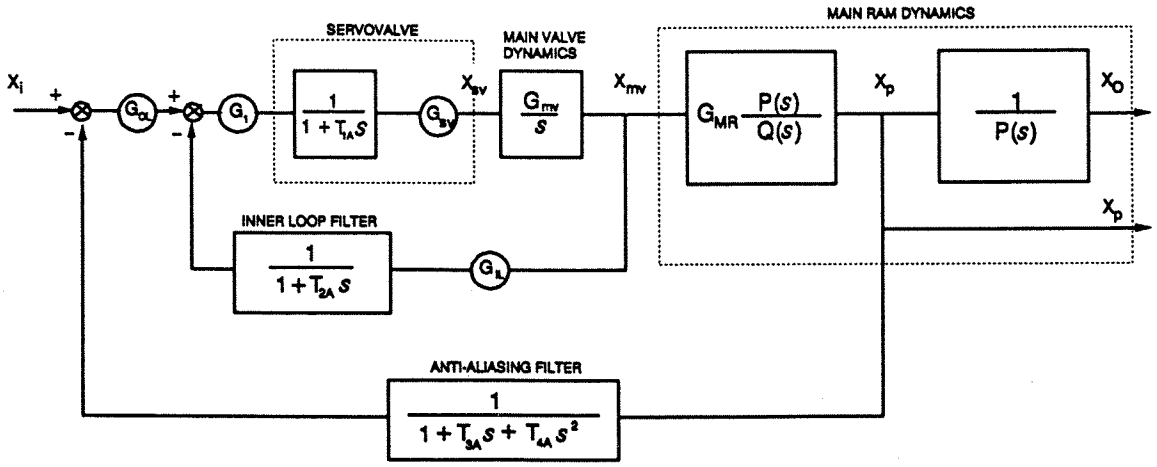

Figure 6 The block diagram of actuation system

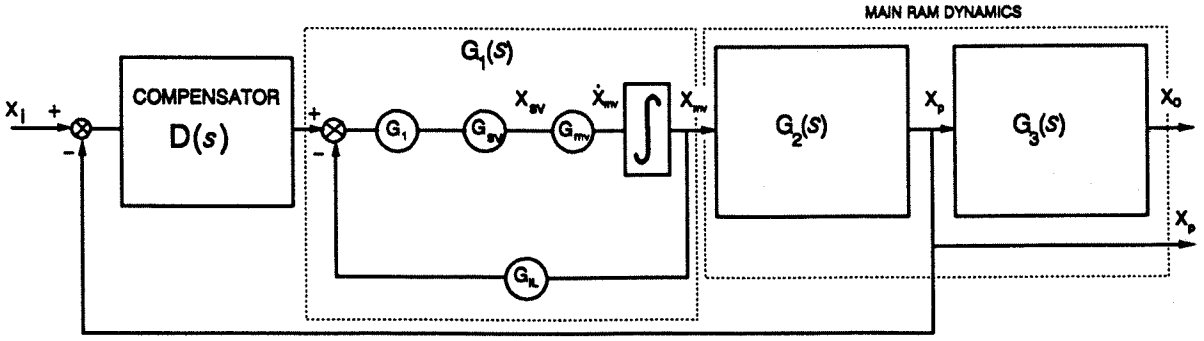

Figure 7 The simplified block diagram of compensated loaded system

The characteristic equation is $1+D(s)G_1(s)G_2(s) = 0$, whose roots are the closed-loop poles of the system. The closed-loop poles can be allocated to the designed positions by varying the compensator gain K. Figure 8 indicates the root-loci of the system with the compensator $D(s)$. The poles and zeros are designated by triangles and circles respectively. The solid lines represent constant damping ratios of $\zeta = 0.707$ and $\zeta = 0.5$. The locus of the roots with increasing K is indicated by arrows. When K = 0, the closed-loop poles are 0, -160.23 and -100±100i on the s-plane. As the value of K is increased from 0 to 1200, the closed-loop poles, at 0 and 160.23, move towards -60. As K is increased from 1200 to 2000, the closed-loop poles break away from the negative real axis, becoming complex and moving towards the imaginary axis. Thus these are the dominant closed-loop poles. However, the closed-loop poles, from -100±100i, move away from the solid line $\zeta = 0.707$ and remain complex throughout the variation of K. A value of K = 1500 is used for the further analysis presented below since this gives a good compromise between closed-loop damping and bandwidth.

Once the compensator is developed, it is used to replace G_{OL} in the model shown in Figure 6. The digital effects are also reintroduced by including a Padé approximation to the sampling to carry out a detailed assessment of the system. The theoretical open-loop frequency response of the compensated system is shown in Figure 9. The crossover frequency of the system with pole-zero compensation is 4.1 Hz compared to 2.5 Hz for the proportional feedback design. The gain and phase margins are 14 dB and 67^0 respectively. No resonant peak appears on the compensated system and the gain rolls off very quickly after 20 Hz. There is also a significant loss of phase at high frequencies.

Having designed and evaluated the compensation scheme using continuous time methods, the compensator is discretized by using pole-zero mapping. This method is utilised because the sampling rate is at least 200 Hz and pole-zero mapping is the simplest to apply computationally and gives reasonable accuracy. The discretized compensator corresponding to the sampling rate 200 Hz is

$$D_1(z) = 1067.355\frac{1-0.9728z^{-1}+0.8649z^{-2}}{1-1.0645z^{-1}+0.3678z^{-2}} \qquad (5)$$

The theoretical continuous time and discretized closed-loop frequency responses of the compensated system are shown in Figure 10, which depicts the frequency response of the main ram with and without the compensation. The solid line is the datum line obtained from the linear model validation. The results of the compensated system indicate that the bandwidth has increased to 9 Hz and the gain magnitude drops rapidly at high frequencies to avoid noise interference. There is no sign of the resonant peak in the compensated system. Also, there is a significant reduction in phase lags at low frequencies up to 5 Hz.

The discretized compensator has then been implemented in the test rig system in real-time. Figure 11 shows the frequency responses of the main ram at sampling rate 200 Hz. The analogue results of the proportional gain G_{OL} show relatively poor bandwidth and phase shift. The compensated system not only increases the bandwidth considerably up to 13 Hz or 15 Hz, but also improves the phase shift below 5 Hz before rolling off rapidly.

Figure 12 indicates the sensitivity of the pole-zero cancellation system by running with hydraulic system number 2 turned off. After the system being compensated, the response shows that the gain magnitude and phase lag at low frequency have been remedied. Despite the dynamic changes, the experimental results indicate that the performance of the system can be maintained.

Multi-loop Feedback Control

State-space Representation of the Actuation System

Apart from the conventional techniques as mentioned in previous section, state-space control design techniques can also be utilised for the design of the digital control system. The Jaguar FBW actuation system can be considered as a single-input/multi-loop feedback linear time-invariant system as shown schematically in Figure 13.

The control signal, $u(n)$ from the digital computer, is a discrete signal. It is also the input to the plant and an input to the estimator. Before being used to control the actuation system, this signal $u(n)$ is passed through a zero-order hold to convert it back to a continuous analogue signal. The continuous control signal, $u(t)$, is conveyed to the servovalves so as to complete the control action. The main valve displacement x_{mv} and the main ram displacement x_p are measurable outputs from the plant. They are sampled by the samplers and then passed to the estimator. Based on the sampled outputs and $u(n)$, the estimator can estimate the full set of system states. To obtain $u(n)$, the input demand is sampled and then compared with feedback signal obtained by multiplying estimates and their corresponding gain values in the control law. The estimator may be either a state estimator (or observer) or a Kalman filter and the control law may be either a pole-assignment control law or an optimal control law.

According to the principle of separation, the control law and the estimator can be designed independently. It is also assumed that no electrical and hydraulic failures are present and the sampling rate is 200 Hz. Thus the discrete state-space representation of the plant is

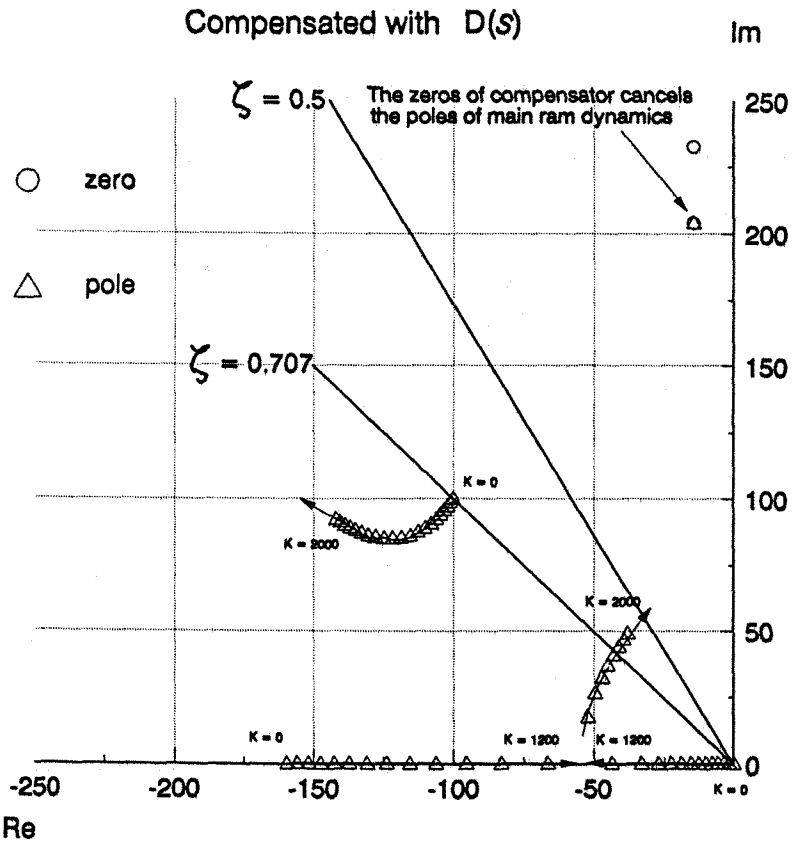

Figure 8 The root-loci as a function of K

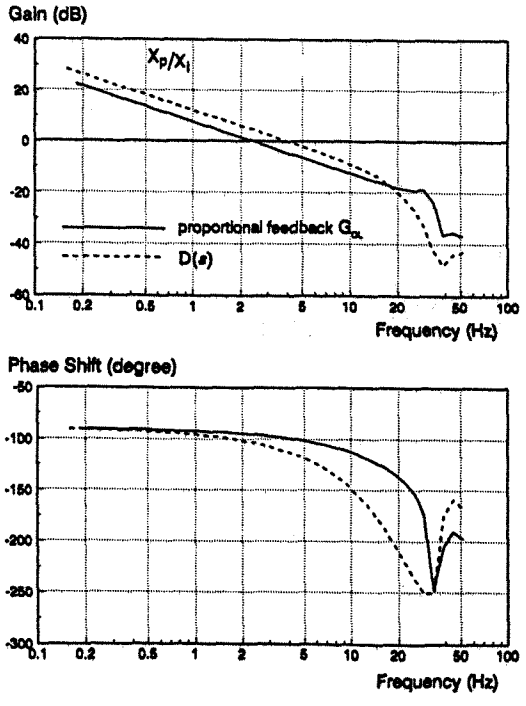

Figure 9 The open-loop frequency response of the compensated system with pole-zero cancellation

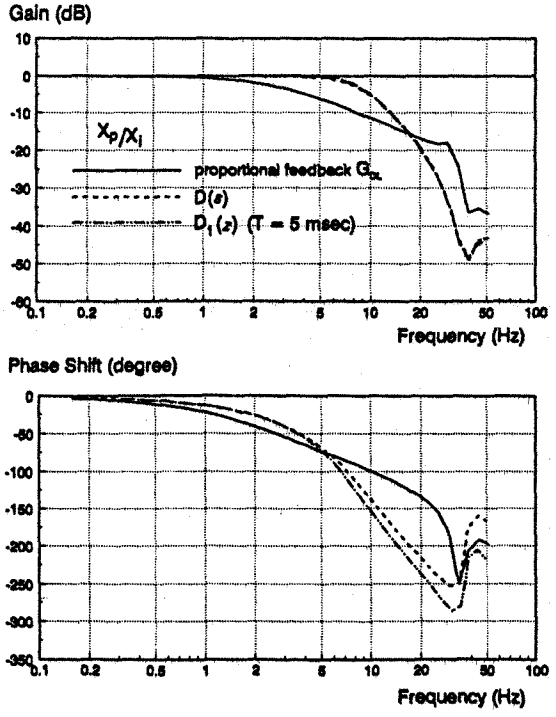

Figure 10 The closed-loop frequency response of the compensated system with pole-zero cancellation

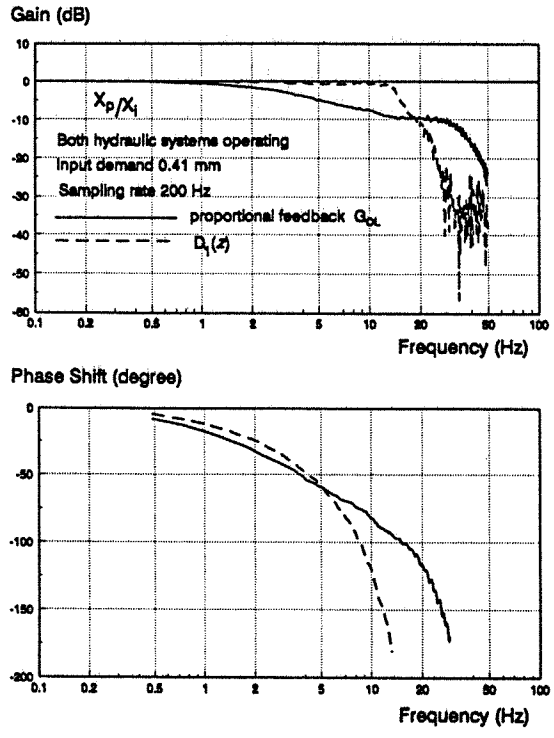

Figure 11 The comparison of the proportional feedback and pole-zero cancellation

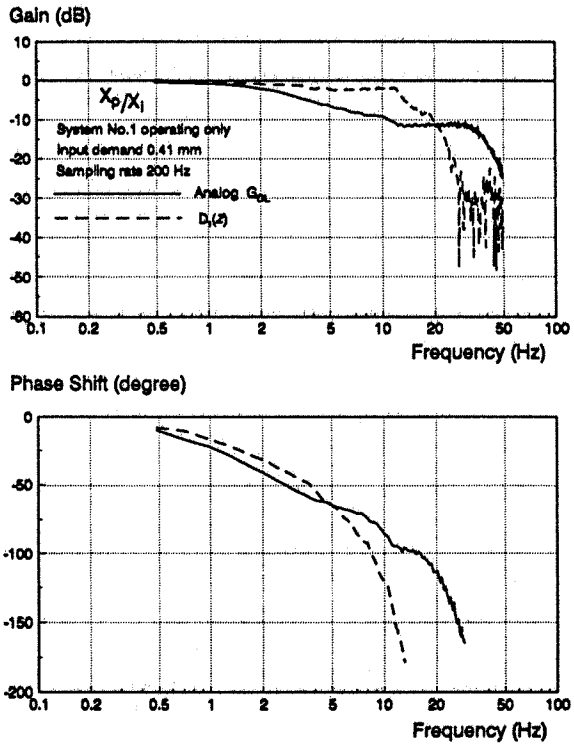

Figure 12 The frequency response of the ram, hydraulic system No.1 operating

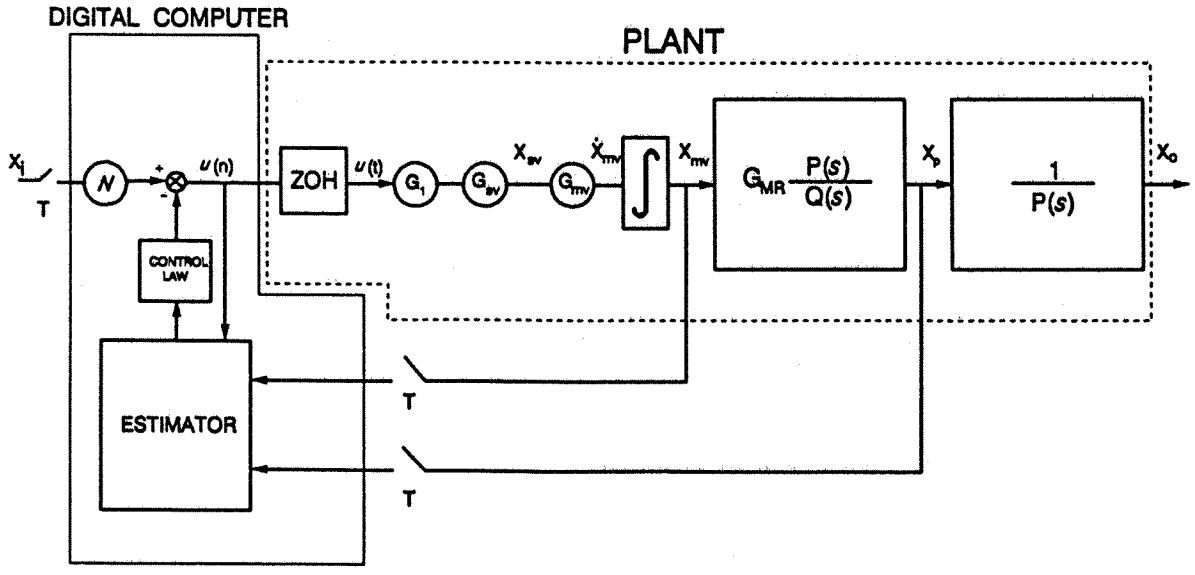

Figure 13 The schematic diagram of single-input/multi-loop output actuation system

$$\mathbf{x}(n+1) = \mathbf{\Phi x}(n) + \Gamma u(n) \tag{6}$$

$$\mathbf{y}(n) = \mathbf{C}\,\mathbf{x}(n) \tag{7}$$

where

$$\mathbf{\Phi} = \begin{bmatrix} 1 & 0 & 0 & 0 \\ 10530.078 & 0.431 & -162.734 & 0 \\ 29.603 & 0.00389 & 0.543 & 0 \\ 0.262 & 2.471\text{x}10^{-6} & 9.497\text{x}10^{-4} & 1 \end{bmatrix}$$

$$\Gamma = \begin{bmatrix} 1.011\text{x}10^{-4} \\ 0.599 \\ 1.046\text{x}10^{-3} \\ 1.296\text{x}10^{-5} \end{bmatrix}$$

$$\mathbf{C} = \begin{bmatrix} 1 & 0 & 0 & 0 \\ 0 & 0 & 0 & 1 \\ 0 & -18.489\text{x}10^{-6} & -5.296\text{x}10^{-4} & 1 \end{bmatrix}$$

Pole-assignment Control Law

At this stage, it is assumed that the complete state $\mathbf{x}(n)$ of the plant can be accurately measured at all times and is available for feedback. Thus the control law is:

$$u(n) = -\mathbf{K}\mathbf{x}(n) + N x_i(n) \tag{8}$$

A reasonable method to select N is that the overall closed-loop gain of the transfer function $X_p/X_i(z)$ at $z = 1$ is 1. Here, according to the analysis, N turns out to be approximately equal to K_4. The system (6) is completely controllable because the controllability matrix is full rank i.e. 4. This implies that the closed-loop characteristic roots of $(\mathbf{\Phi} - \mathbf{\Gamma K})$ can be arbitrary located in the complex plane by choosing $\mathbf{K}$ suitably. Since the open-loop system is single-input, $\mathbf{K}$ is a row matrix which is unique for a set of specified eigenvalues of the closed-loop system.

Figure 14 shows the simulation closed-loop frequency responses of X_p/X_i for the different $\mathbf{K}$ matrices listed in Table 1. In Figure 14, the solid line is the proportional feedback analogue system which has been used for mathematical validation. The peak in the response of the proportional feedback system response is due to the control surface resonance. The poles of the resonance in the z-plane are $z = 0.487 \pm 0.793i$ while the trough due to a pair of complex-conjugate zeros, $z = 0.37 \pm 0.85i$.

Referring to the curve A, a pair of complex-conjugate closed-loop poles is allocated to cancel the existing pair of complex-conjugate zeros and then another new pair of complex-conjugate poles are allocated to $z = 0.88 \pm 0.078i$. The peak and the trough disappear as shown in Figure 14.

In the cases used to produce curves B and C the closed-loop poles are assigned to suitable locations in order to give sufficient bandwidth and damping to the system. Curves B and C in Figure 14 still show the trough in the gain response.

The three curves A, B and C can improve bandwidth; the gains for curve C gives the best bandwidth. As far as the phase shift is concerned, curve C shows an improved phase lag up to 10 Hz, whilst curve A shows an improvement up to 2.2 Hz and curve B only up to 1 Hz.

Steady-state Optimal Estimation (Kalman filter)

The control law designed in previous section assumed that all the states were available for feedback. However, the states x_o and $\dot{x}_o$ are not measurable in practice. The purpose of this section is to develop an estimator to reconstruct all the states of the actuation system from the measurements x_{mv} and x_p. The most appropriate estimator is a Kalman filter.[11],[12]

In the development of the equations for the Kalman filter process and measurement noise are assumed to be present in the system. Thus Eqs. (7) and (8) can be modified as follows:

System model

$$\mathbf{x}(n+1) = \mathbf{\Phi x}(n) + \Gamma u(n) + \mathbf{w}(n) \quad \mathbf{w}(n) \sim \mathrm{N}(0, \mathbf{Q}_w)$$

Measurement model

$$\mathbf{y}_1(n) = \mathbf{C}_1 \mathbf{x}(n) + \mathbf{v}(n) \qquad \mathbf{v}(n) \sim \mathrm{N}(0, \mathbf{R}_v)$$

where the process noise $\mathbf{w}(n)$ and measurement noise $\mathbf{v}(n)$ are assumed to have zero mean, to be white and Gaussian. The matrix $\mathbf{C}_1$ is also modified to include only the measurements of x_{mv} and x_p

i.e. $$\mathbf{C}_1 = \begin{bmatrix} 1 & 0 & 0 & 0 \\ 0 & 0 & 0 & 1 \end{bmatrix}$$

The Kalman filter algorithm in steady-state is as follows:

$$\bar{\mathbf{x}}(n+1) = \mathbf{\Phi}\hat{\mathbf{x}}(n+1) + \Gamma u(n) \tag{9}$$

$$\hat{\mathbf{x}}(n) = \bar{\mathbf{x}}(n) + \mathbf{L}_\infty \left[\mathbf{y}_1(n) - \mathbf{C}_1 \bar{\mathbf{x}}(n) \right] \tag{10}$$

where $\hat{\mathbf{x}}$ is the vector of state estimates and is required for the feedback. The steady-state Kalman gain $\mathbf{L}_\infty$ for this actuation system can be determined by the relative importance of elements of $\mathbf{Q}_w$ and $\mathbf{R}_v$, which are chosen empirically to be:

$$\mathbf{Q}_w = \begin{bmatrix} 1 & 0 & 0 & 0 \\ 0 & 1 & 0 & 0 \\ 0 & 0 & 1 & 0 \\ 0 & 0 & 0 & 1 \end{bmatrix} \quad \text{and} \quad \mathbf{R}_v = \begin{bmatrix} 1 & 0 \\ 0 & 1 \end{bmatrix} \tag{11}$$

The steady-state Kalman filter gain is given to be

$$\mathbf{L}_\infty = \begin{bmatrix} 0.6154 & 0.0294 \\ 2083.4 & -173.87 \\ 12.07 & 6.219 \\ 0.0294 & 0.629 \end{bmatrix} \tag{12}$$

It is useful to test this algorithm experimentally over a range of initial conditions to see how well the filter can converge to match the actual system response. Typical results taken from the test rig are shown in Figure 15. These show the estimate of x_{mv} overshoots slightly and then follows the actual x_{mv}. There is no overshoot on x_p and the estimate x_p converges rapidly to the actual behaviour. The Kalman filter estimator can thus provide good estimates of the system states.

This Kalman filter can then be combined with pole-assignment control law to form a controller. In the following results the pole-assignment case A referred to previous section is used. The controller gains are thus

$$\mathbf{K} = \begin{bmatrix} 3599 & 0.18 & -11.1 & 798 \end{bmatrix} \tag{13}$$

and the Kalman gain is as above. The rig performance of the digital control with both hydraulic systems operating is illustrated in Figure 16, where the result of an optimal controller is also taken for comparison.[6] The results show that the pole-assignment plus Kalman filter gives the best bandwidth around 13 Hz. The optimal control can also improve the bandwidth as compared with the analogue one. In phase shift, the optimal control shows the worst phase lag throughout the frequency range. For the pole-assignment plus Kalman filter, there is a reduction of phase lag up to around 2.2 Hz before crossing the analogue result. The analogue control can still maintain lower phase shift at high frequencies.

The sensitivity of the digital controller was also tested by running hydraulic system No.1 only as shown in Figure 17. The pole-assignment plus Kalman filter still gives the best bandwidth up to around 13 Hz. As far as the phase shift is concerned, there is a noticeable reduction of phase shift of pole-assignment plus Kalman filter result at low frequencies.

Simulation of Controller (Pole-assignment plus Kalman Filter) on Loaded Model

Sensitivity of The Feedback Gains and System Parameters

In the experiments it was found that the control gains obtained from the theory needed to be tuned slightly so as to give better performance. In addition, the system performance may be affected by the variation of the system parameters such as the valve flow coefficient.[4]-[6] Their effects to the system performance were investigated theoretically by incorporating the pole-assignment control law plus the Kalman filter into the nonlinear model of the actuation system.[6]

Figures 18 and 19 show the sensitivity of the feedback gains and system parameters on the nonlinear model respectively. A nominal gain was chosen to be $\mathbf{K}$ = [3599 0.18 -11.1 798] as listed in Table 1. From Figures 18(a) to (d), the elements of the nominal control gain are varied by a certain percentage in turn. The results of the linear model using the nominal gain are also superimposed on the figures for comparisons only. The results show that, in gain magnitude, the nonlinear result with the same nominal gain matches the linear result at low frequency, but from about 10 Hz onward it is clear that the nonlinearities must be included if gain is to be represented accurately. For the phase shift, the nonlinear results are similar to the linear one up to 20 Hz.

The results in Figure 18(a) show that the system bandwidth can be improved by decreasing the nominal gain K_1 until it is reduced by more than 20% but this causes the system to have a resonance peak. There is also a noticeable reduction of phase lag at low frequency up to 4.5 Hz as the gain is reduced, but the system suffers an increase in phase lag beyond that frequency. The variation of K_2 as shown in Figure 18(b) indicates that there is no distinctive change in bandwidth and the curves start to deflect away from the nominal at about 5 Hz. The curves in phase shift begin to diverge slightly at 2 Hz and then converge together at 20 Hz and then diverge again. The change in phase shift in the region 2 Hz to 20 Hz is only slightly away from the nominal although K_2 is increased and decreased by more than 20%. In Figure 18(c), by increasing the nominal gain K_3, the bandwidth of the system and the reduction of phase lag at low frequency can be improved but only slightly, and not as much as by the reduction of K_1. The curves in gain magnitude converge at 20 Hz while the

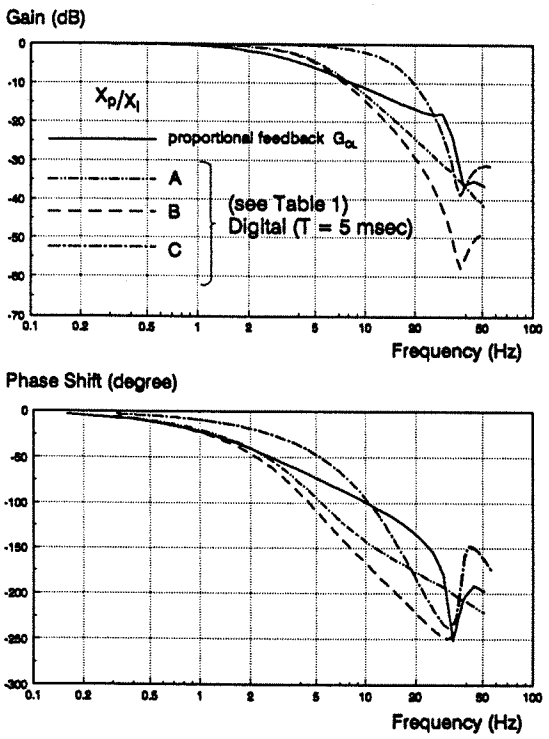

Figure 14 The closed-loop frequency responses using pole-assignment control law

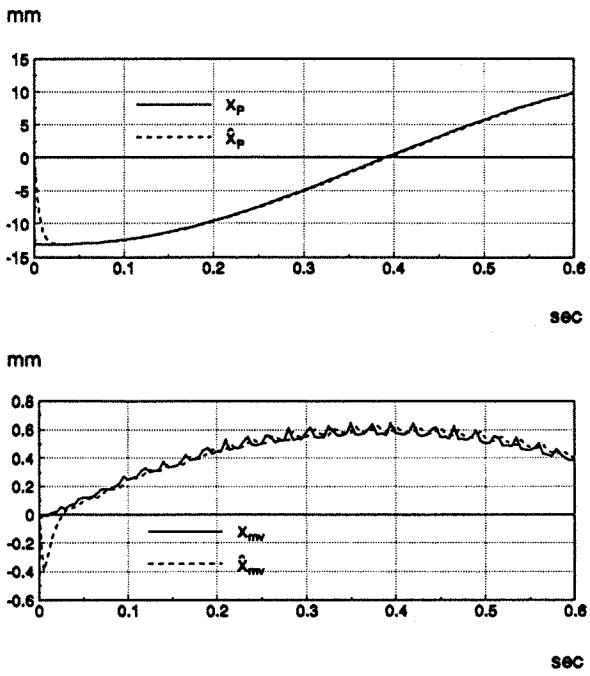

Figure 15 The tracking of the measurement outputs using Kalman filter

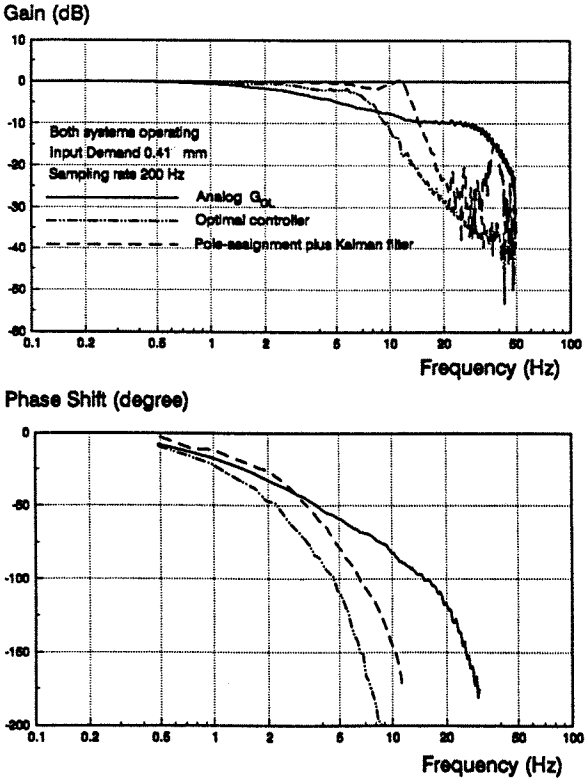

Figure 16 Comparison of digital control and analogue results for both hydraulic systems operating

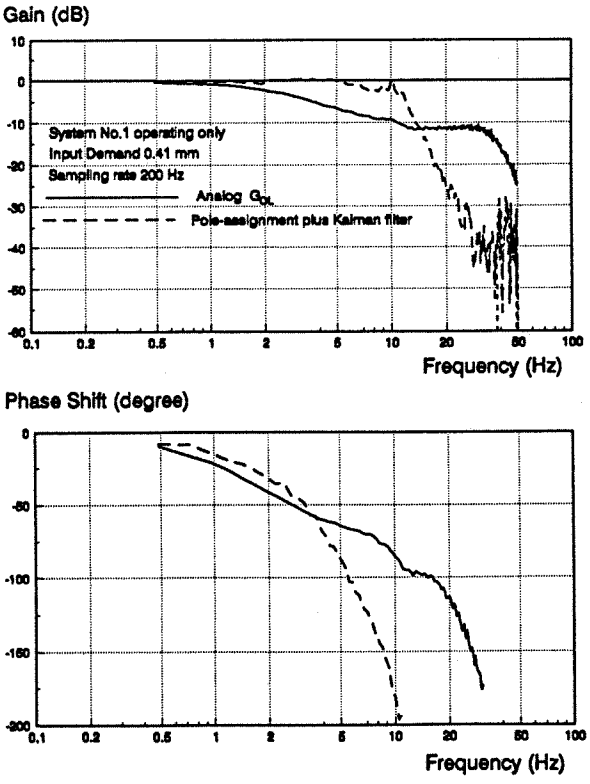

Figure 17 Comparison of digital control and analogue results for hydraulic system No.1 operating

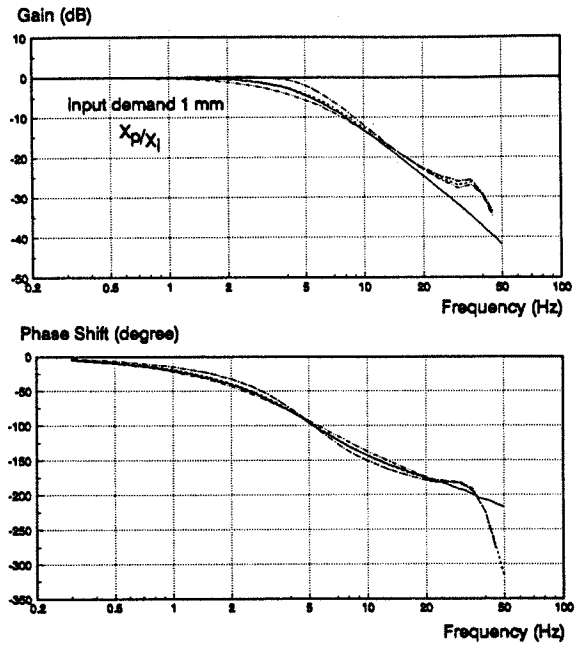

(a) The variation of K_1

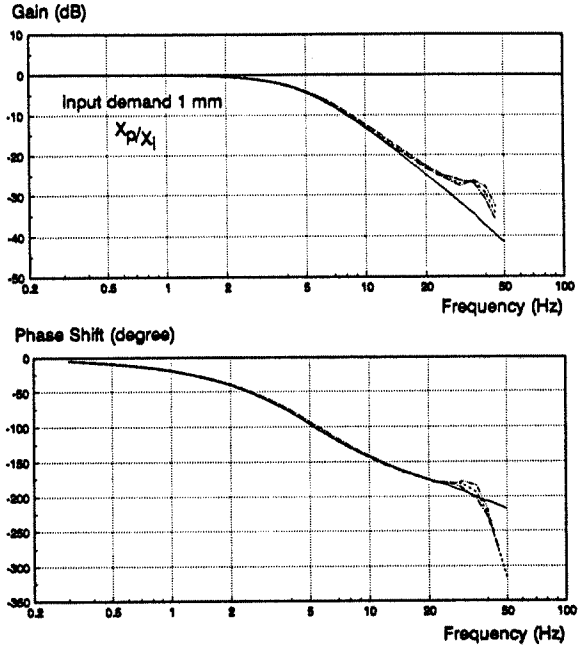

(b) The variation of K_2

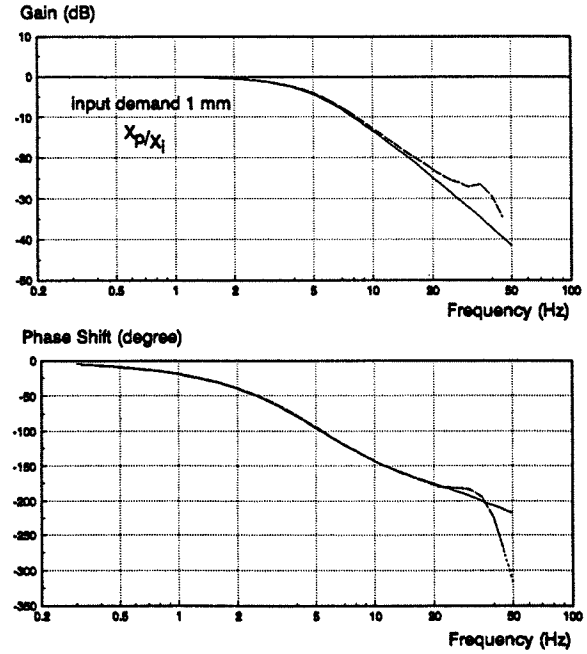

(c) The variation of K_3

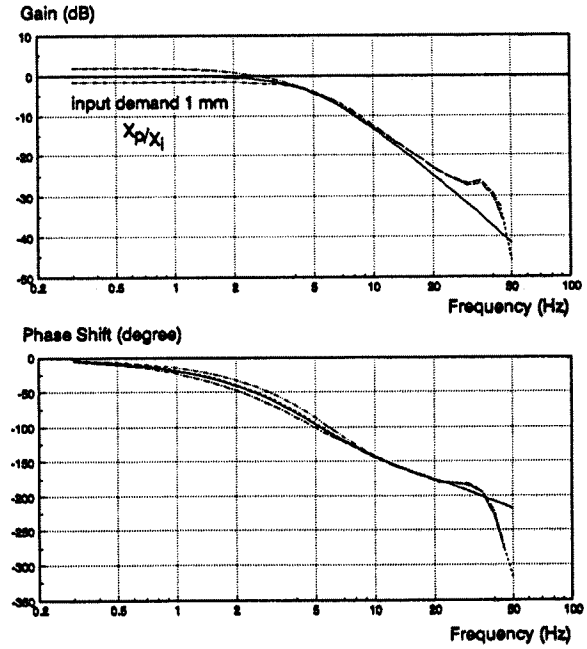

(d) The variation of K_4

linear model, nominal

nonlinear model, nominal

+20%

-20%

Figure 18 The sensitivity of the nonlinear model to feedback gains

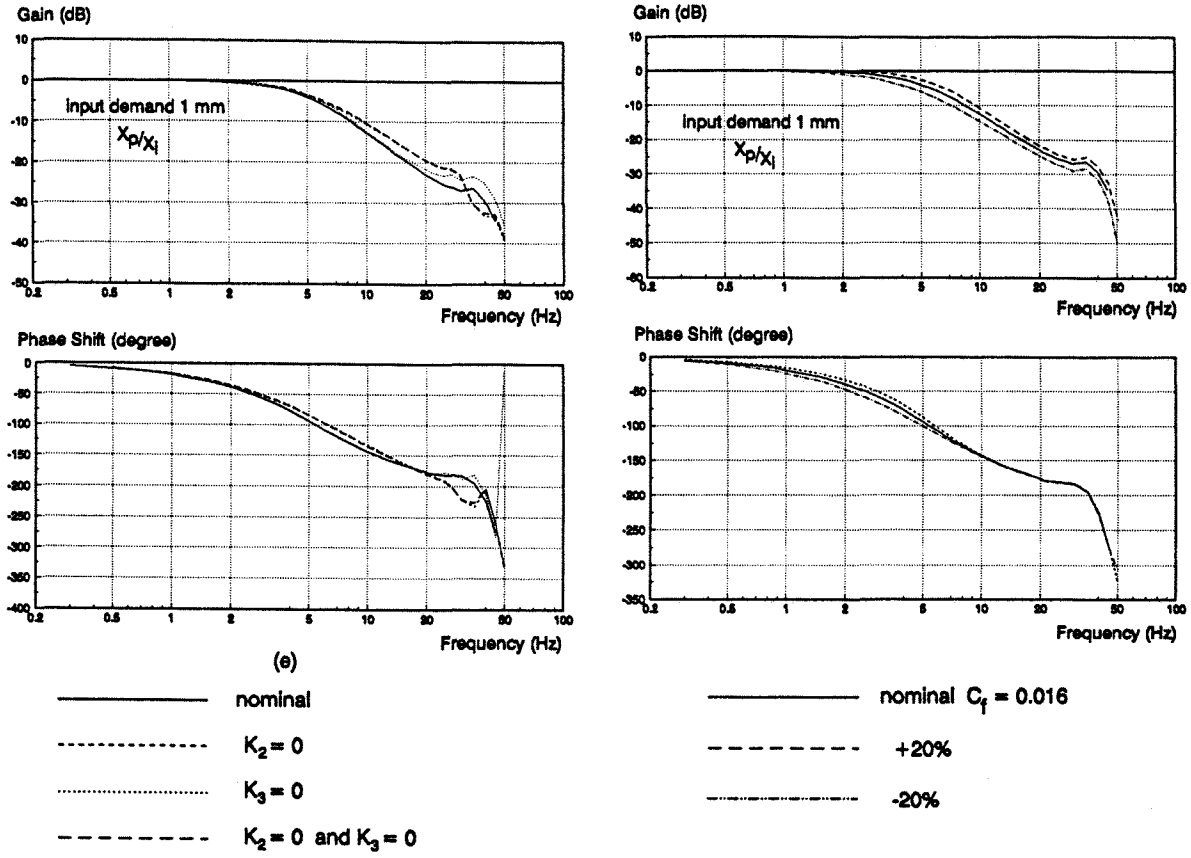

Figure 18(cont'd) The sensitivity of the nonlinear model to feedback gains

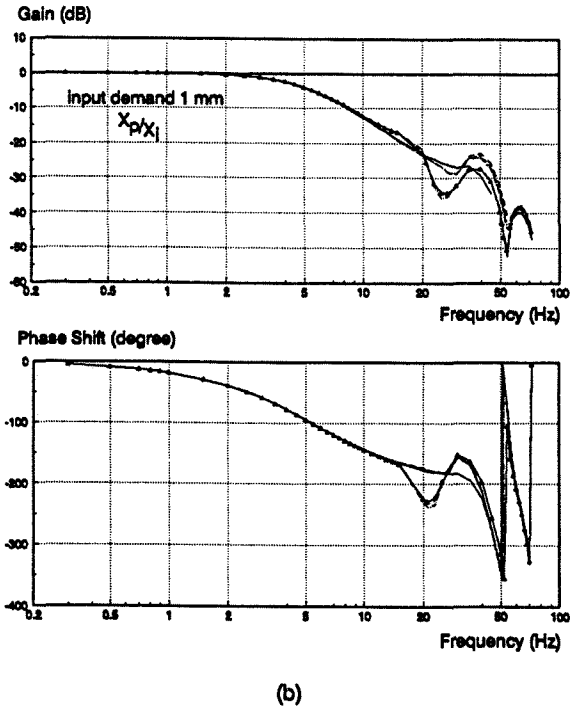

line style	ζ_c	ω_c (Hz)
———	0.07, nominal	35, nominal
- - - - -	nominal	+40%
.....	nominal	-40%
- - - - - -	-40%	+40%
—·—·—	-40%	-40%
—··—··—	+40%	+40%
——△——	+40%	-40%

Figure 19 The sensitivity of the nonlinear model to system parameters

curves in phase shift converge at 4.5 Hz and then diverge. The variation of K_4 in Figure 18(d) illustrates that, in gain magnitude, the curves go up or down by reducing or increasing the gain respectively. It is interesting that a reduction of phase lag is possible by increasing the gain at low frequency.

The variations introduced here to the gains K_1 and K_4 would allow for errors between theoretically preferred values and the effective values in a real system. In practice, these two represent the gains in the inner and outer loop feedback respectively, but the real-time control algorithm will use products and quotients of several gains and the total effective loop gain will not appear as a simple constant. The values of K_1 and K_4 will be chosen, in some sense, to compensate for these other factors and if changes occur in such factors, over time, so also must the values of **K** be changed to keep the system performance constant. For testing purposes, it is obvious that direct changes of K_1 and K_4 are a convenient alternative to varying a selection of contributory factors.

When the experiments were carried out, the oscillation of the system was encountered by setting either $K_2 = 0$ or $K_2 = 0$ and $K_3 = 0$. The phenomenon can be explained in Figure 18(e). The resonance peak appears at around 35 Hz. In practice, the resonance peak could become very dominant if the main ram gain in the forward path was increased.[5],[6] In practice, this gain is a function of several factors such as the valve flow coefficient, the port geometry, the hydraulic supply pressure and the piston area. Indeed just the flow coefficient will depend on pressure drops, local valve dimensions and operating frequency.[5],[6] Whilst several of these can change, over time, perhaps due to normal wear, it is convenient to look at possible changes of value in any factor of the main ram gain by using variations in the flow coefficient alone. In Figure 19(a), the effect of this coefficient on the system performance, with the same controller as above, is investigated. The results show that the bandwidth and the reduction in phase lag at low frequency can be improved with an increase in valve flow coefficient.

Two other conveniently changeable system parameters are damping and hydraulic stiffness. The former varies if there is leakage inside the valve and piston cylinder. The latter depends on the bulk modulus of the hydraulic fluid, on the geometry of the piston/cylinder, and on the number of hydraulic systems operating. In turn, these affect the resonance frequency. Their effect on the system performance is shown in Figure 19(b). The change in damping of the system can be represented by a variation of the damping ratio ζ_c, while the change in resonance frequency is brought about by a change in hydraulic stiffness or inertia load or both.[6] (The resonance frequency is determined by the square root of the ratio of total stiffness to inertia load.) In these simulations, the variations of the damping ratio and resonance frequency by means of changing inertia load are exaggerated so as to see noticeable changes of the system performance. The results in Figure 19(b) show that the bandwidth and phase lag at low frequency are hardly affected by these parameters even for changes of ±40%.

The table in Figure 19(b) provides a reminder that the natural uncontrolled system had a pair of poles at about 35 Hz, but the solid line in the gain and phase plots shows a smooth variation of the both at that frequency. It is important to recognize that this smoothness hides the pole-cancellation. If either of the two parameters ζ_c or ω_c is changed, that cancellation fails and a new response must be recognized. As the inertia is reduced, a new higher natural frequency is made evident by a new resonance peak at about 40 Hz, whereas a high inertia leads to an anti-resonance near 20 Hz. The changes in phase seen in Figure 19(b) are consistent with these movements of characteristic roots and the magnitudes of peaks or troughs in both gain and phase are understandably dependent on the values of the damping ratio.

All nonlinear results in Figures 18 and 19 indicate that the variations of feedback gains and system parameters in the nonlinear model have much the same as they do in the linear model.[6]

Simulation of Impedance Test

The actuator ram is normally subject to applied loads from the control surface when the actuator is mounted between the airframe and the control surface. The ability to resist these loads is described by its stiffness, which can be expressed in terms of a frequency dependent gain and phase. This complex stiffness is referred to as the actuator impedance and has a profound effect on certain aspects of the aircraft dynamics, particularly flutter. As a result, the effectiveness of the controller on the impedance test needs to be evaluated.

The impedance is defined more precisely as the ratio of dynamic applied load to dynamic displacement, where these are the external load at the output end of the actuator, with no inertia load, and the displacement of the same end. It should be noticed that although the applied external load is oscillatory, it can have a steady component. In the simulation, it is straightforward to set the inertia load small enough to represent the loading mechanism, through which the external force is applied. The ram/body impedance (F_E/X_p)results for the applied dynamic load of 0±4448 N, 0±8896 N and 0±13344 N are shown respectively in Figures 20(a), (b) and (c). The simulation results obtained from the digital loop closures are compared with those obtained from the original analogue control design. They only show the ram/body stiffness with the starting frequency 10 Hz. However, in theory, they give infinite stiffness at zero frequency

because of the ram position feedback. When the curves cross the real part (imaginary part is zero) at low frequencies, the digital results shows lower stiffness (by about half) than the analogue ones. Thus greater consideration needs to be given to the effects of the controller on the elastic behaviour of the aircraft.

Discussion and Conclusions

A simplification of the linear mathematical model has been used to derive a simple pole-zero cancellation compensator. The experimental results show a significant increase in bandwidth and a reduction in the phase lag at low frequency.

In real situation the exact pole-zero cancellation cannot occur, for example, in the case of the aircraft actuator, the aerodynamic hinge moment and damping characteristics change with flight condition. In addition, the discrepancies may be caused by the modelling errors and parameter changes during operation. Investigation of the problems, which may arise from actuator parameter changes, indicates that the poles do not move sufficiently to cause problems. It has been demonstrated by running the hydraulic lane independently, the experimental results show that the performance of the system can still be maintained.

An alternative approach utilising a Kalman filter and pole-assignment for the controller design has also been tested. Initial results presented also show an increase in bandwidth and a reduction in low frequency phase lag. The experimental results also indicate that there is no lack of robustness due to parameter changes. The simulation results show that the variation of feedback gains, K_1 and K_4, or the valve flow coefficient could significantly affect the bandwidth and reduction of phase lag at low frequency. The setting of $K_1 = 0$, which amounts to preventing any feedback from the acceleration of the inertia load, has a strong influence on the gain and phase. Further testing is required to evaluate pole-assignment case C which shows the best performance in theory. Evaluation with a comprehensive nonlinear model shows encouraging results.[6]

The performance benefits gained from these two design techniques are compared with the optimal control and original design as shown in Figure 21. The results show that the pole-zero cancellation achieves the highest bandwidth, 14.4 Hz, and the pole-assignment plus Kalman filter, 12.7 Hz. The optimal controller can also achieve a bandwidth up to 6.8 Hz better than the original design, which gives 3.7 Hz. As far as the phase shift is concerned, all the results are compared at discrete frequencies. The optimal controller suffers the worst phase loss at this frequency range but the pole-assignment plus Kalman filter controller shows a phase improvement up to 2.2 Hz. The pole-zero cancellation system gives improved phase lag up to 5.1 Hz. This would indicate that for the systems evaluated so far the pole-zero cancellation approach gives better results. However, further improvements in the performance of the Kalman filter plus pole-assignment controller can be expected when the control law case C is evaluated.

Both of the designs evaluated show larger phase lags at high frequency than the original proportional feedback control law. However, this is unlikely to influence the handling qualities of a flight control system. Further investigation of the integration of an actuator with this characteristic in an aircraft system is required.

The feedbacks introduced by the two approaches can be related to pressure and force feedbacks. Feedbacks of this type are known to influence the actuator impedance. In the case of pole-assignment plus Kalman filter, the impedance simulation shows that this control system produces an impedance that is less stiff than the original as seen when under analogue control.

Acknowledgements

The authors would like to thank Dr.R.Stirling and Dr.D.L.Birdsall for their valuable advice throughout the present work. Thanks are also due to the Science and Engineering Research Council, U.K. and Dowty Aerospace Wolverhampton for supporting this work.

References

(1) Burrows, C.R., *Fluid Power Servomechanisms.* Van Nostrand Reinhold, 1972.

(2) Ezekiel, F.D., The effect of conduit dynamics on control-valve stability. *Trans. ASME*, Vol. 80, pp.904 - 908, 1958.

(3) Ainsworth, F.W., The effect of oil-column acoustic resonance on hydraulic valve "squeal". *Trans. ASME*, Vol. 78, pp. 773-778, 1956.

(4) Chun, L.H.L. Rig test validation of a mathematical model of the Jaguar FBW taileron actuator with no load. *Dept. of Aero. Eng. Report No.430, University of Bristol*, October 1991.

(5) Chun, L.H.L. Rig test validation of a mathematical model of the Jaguar FBW taileron actuator with loading inertia on the ram. *Dept. of Aero. Eng. Report No.439, University of Bristol*, March 1992.

(6) Chun. L.H.L. The design and test rig evaluation of advanced control laws for primary flight control actuators. Ph.D. Thesis University of Bristol 1993.

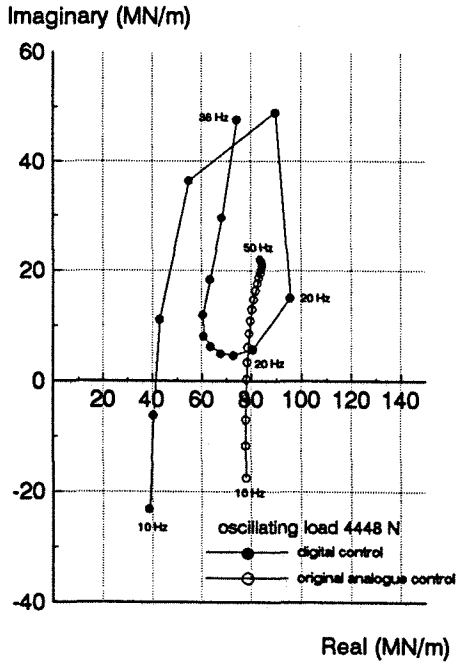

(a)

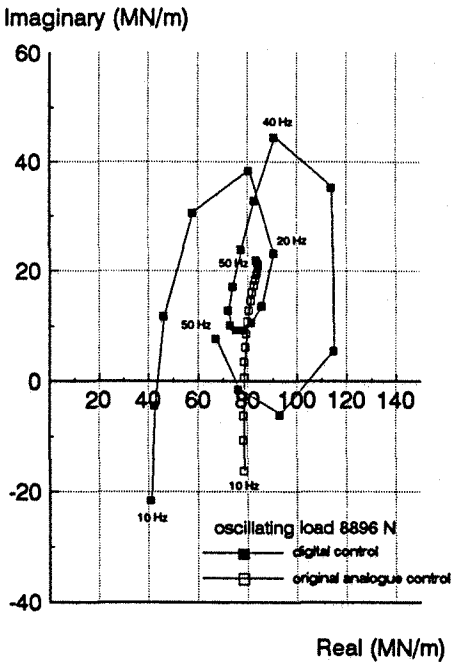

(b)

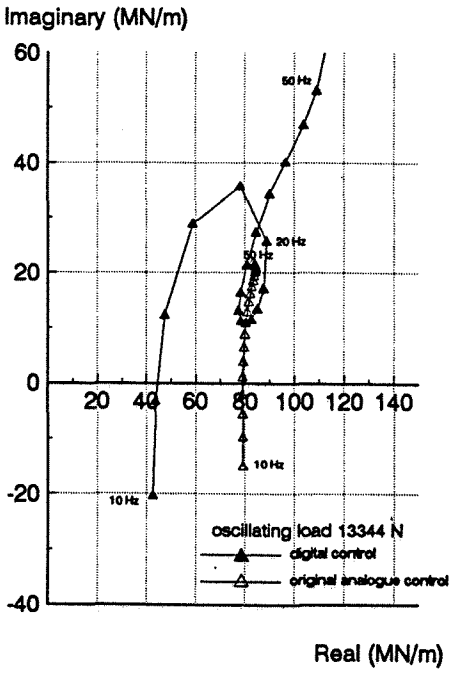

(c)

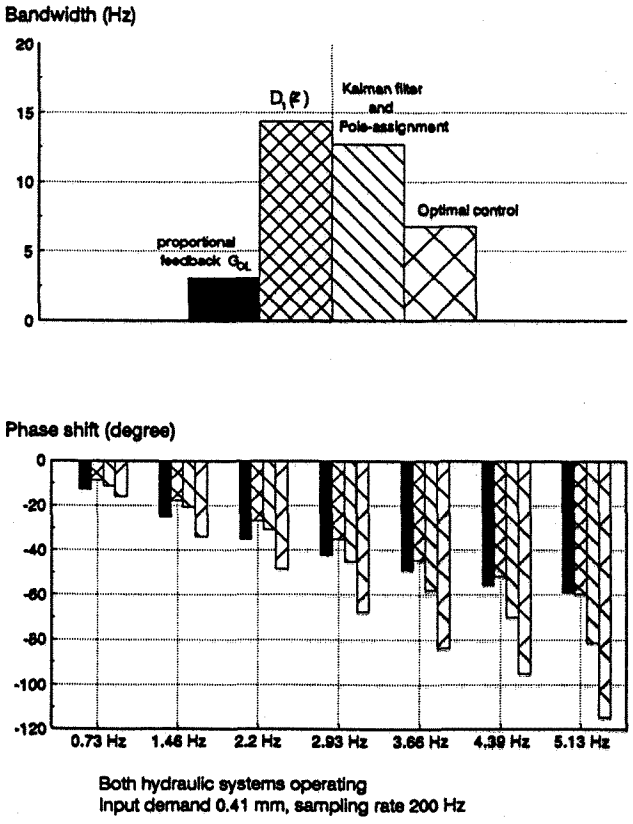

Figures 20(a), (b) and (c) Actuation system impedances

Figure 21 Comparison of performance benefits

(7) Data Translation User Manuals DT2801-series and DT2821, 1988/1989.

(8) Stirling, R. Simulation of a digital aircraft flight control system. *Simulation*, May 1983.

(9) Ogata, K. *Modern Control Engineering*. Prentice-Hall, Englewood Cliffs, 1970.

(10) Kuo, B.C. *Automatic Control Systems*. Prentice-Hall, Englewood Cliffs, 1975.

(11) Franklin, G.F., Powell, J.D. and Workman, M.L. *Digital Control of Dynamic Systems*. Addison-Wesley, 1980.

(12) Anderson, B.D.O. and Moore, J. *Optimal Filtering*. Prentice-Hall, Englewood Cliffs, N.J., 1979.

Table 1 Pole-assignment control gains

curve	closed-loop poles in *s*-plane	closed-loop poles in *z*-plane	**K**
A	-14.32±232.12i, -25±17.77i	0.37±0.85i, 0.88±0.078i	[3599, 0.18, -11.1, 798]
B	-25±17.77i, -300, -400	0.88±0.078i, 0.223, 0.135	[10424, -0.11, -131.3, 476]
C	-80±80i, -150, -300	0.62±0.26i, 0.472, 0.223	[10797, 0.01, -89.6, 3010]